Northumbria Research Link

Design Methodology for Six-Port Equal/Unequal Quadrature and Rat-Race Couplers with Balanced and Unbalanced Ports Terminated by Arbitrary Resistances

Lingxiao Jiao, Yongle Wu, Weiwei Zhang, Mingxing Li, Yuanan Liu, Quan Xue, and Zabih Ghassemlooy

Abstract—For the first time, the six-port quadrature and rat-race couplers with balanced-unbalanced-hybrid ports are proposed. The corresponding design methodology is presented, which is capable of designing the proposed couplers with arbitrary power divisions and terminated resistances. In this paper, four types including quadrature and rat-race couplers are fully analyzed, covering all the application configurations of the balanced/unbalanced ports. Besides, the design equations are rigorously derived, with the final design procedures presented. Eventually, prototypes of the four coupler types are fabricated and experimentally measured. The final results sufficiently validate the proposed methodology.

Index Terms—Balanced circuit, balanced-to-unbalanced circuit, coupler, quadrature, rat-race.

I. INTRODUCTION

THE RECENT trends of the RF/microwave circuit are the increasing complexity, integration and power efficiency. With circuits becoming more complex and packaging more functionalities, the device density is greatly increased, which leads to severe electromagnetic interactions between the circuit nodes. Moreover, as a side effect for pursuing high power efficiency, the interference and crosstalk from the mutual coupling and environmental noise become significant due to the low-level excitation voltages. Therefore, the concept of balanced circuits, also known as the differential one, is introduced for overcoming the aforementioned shortfalls of single-ended circuits, owing to its high immunity to the common-mode signals.

To develop high-performance balanced systems, a growing research activities on the component level are reported, in-

cluding filters [1]–[3], power dividers [4], [5], couplers [6]–[8], duplexers [9], and antennas [10]. All those components are considered as fully-balanced structures, which are only suitable in balanced systems. However, since balanced circuits achieve common-mode suppression at the cost of nearly twice the number of devices, the single-ended systems are still indispensable when considering both the circuit size and performance. Conventionally, to convert a balanced/unbalanced port to an unbalanced/balanced one, baluns or other components with similar function are used. However, this approach is contrary to our intention of reducing the number of devices in the circuit. As a consequence, the balanced-to-unbalanced components are important when connecting the existing single-ended systems and the emerging balanced systems. This is because they are free from the cascaded baluns. Therefore, apart from the fully-balanced configuration, a large number of components with unbalanced/balanced-hybrid ports are proposed. For example, 5-port power dividers with an unbalanced input and balanced outputs are proposed in [11], [12], and 4-port power dividers with a balanced input and unbalanced outputs are reported in [13]–[15]. In addition to power dividers, balanced-to-unbalanced (or vice versa) duplexers and filters (also known as the filtering balun) are also presented in [16] and [17]–[19], respectively. Nevertheless, couplers with balanced and unbalanced ports are still untouched, including both the quadrature and rat-race types.

As a fundamental and indispensable component, the coupler with balanced-unbalanced-hybrid ports should not be absent when building a balanced system. Considering 6-port quadrature couplers with two balanced and unbalanced ports, there are four types based on different port configurations as shown in Fig. 1(a). Referring to Fig. 1(a), the topologies I and II represent the coupler with a balanced and unbalanced coupled or through output, while the input or isolation port is balanced/single-ended. Whereas, the topologies III and IV show the configurations with balanced and unbalanced outputs, respectively. The rat-race couplers have similar topologies, see Fig. 1(b). For the coupler of branch-line type, due to its symmetry nature [20], the topologies I and II, III and IV in Figs. 1(a) and 1(b) can be merged into one. For example, let's consider a Doherty power amplifier in a balanced system, as shown in Fig. 2, where balancing is only needed at the input and output stages. It is expected that the transistor stage is still a single-ended structure, where only two amplifier devices
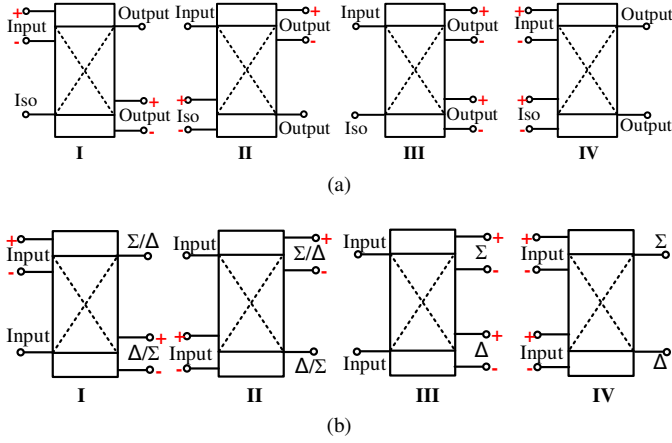
Fig. 1. Topologies of quadrature and rat-race with different balanced-unbalanced port sets: (a) Quadrature coupler; (b) Rat-race coupler.
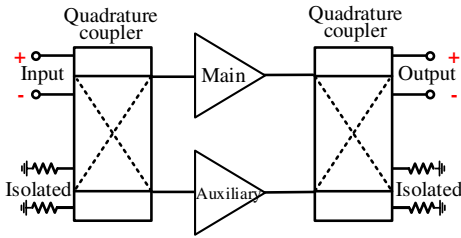

Fig. 2. Example of the proposed-coupler application: a Doherty power amplifier applied in balanced systems.

Fig. 3. Two balanced-to-unbalanced quadrature couplers: (a) Type 1, and (b) Type 2.
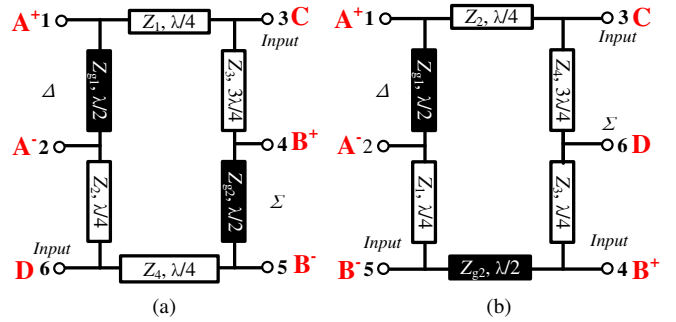
Fig. 4. Two balanced-to-unbalanced rat-race couplers: (a) Type 1, and (b) Type 2.

are needed. At the balanced input and output stages, there are two quadrature couplers corresponding to IV in Fig. 1(a). For optimal performance, the unequal power divisions and impedance transformations may be needed for the quadrature couplers.

In this paper, for the first time, we propose a design methodology for 6-port branch-line couplers with balanced and unbalanced ports, including both the quadrature and rat-race types. The proposed couplers can be used for connecting balanced and unbalanced circuits, while rejecting the common-mode interferences. We present rigorous design equations, detailed design procedure, and verification prototypes of the proposed coupler. Overall, the proposed couplers have many exceptionally-good characteristics including the followings:

1) *Single component*: The coupler is able to connect balanced and unbalanced systems while maintaining the coupler's functionality. Only a single component is needed, with no cascaded baluns. The co-design offers flexibility and relatively-simple optimization.
2) *Multi-functional*: The proposed methodology enables designing couplers with arbitrary power division (as in [21]) and terminated resistances (as in [22]).
3) *Universal*: The design methodology is based on the basic transmission-line theory, which is compatible with various technologies including printed circuit board (PCB), integrated circuits (IC), low-temperature co-fired ceramic (LTCC), *etc.*, whether uniplanar, single-layer or multi-layer.
4) *Simple*: The design equations are simple and analyt-

ical, which facilitates the process for computer-aided designs.
5) *Improved performance*: Under the differential mode, the balanced-to-single-ended coupler operation is complete and effective, while the common-mode signals are completely suppressed.

To conclude, the proposed couplers with balanced and unbalanced ports could be an essential part of building balanced-circuit systems.

II. THE SCHEMATIC AND DESIGN THEORY

The schematic of the proposed four types of quadrature and rat-race couplers are shown in Figs. 3 and 4, respectively. All four types are simply composed of branches of $\lambda/2$, $\lambda/4$, or $3\lambda/4$ lengths, where λ is the wavelength. The four types could cover all applications shown in Figs. 1(a) and 1(b).

The following sections will show the detailed analysis for designing the four coupler types. The analyses begin with the standard single-ended S matrices, which are directly converted from the Y matrices of Figs. 3(a), 3(b) and Figs. 4(a), 4(b). Next, the standard S matrices are converted to the mixed-mode S parameters. Finally, the obtained mixed-mode S parameters are compared with the ones from the expected performance, and then related equations are established. Following solving these equations, the final design formulas will be derived.

A. The Mixed-Mode S Matrix

First, we designate ports A and B as the balanced ports, while ports C and D as the single-ended ports as Figs. 3

TABLE I
CORRESPONDENCE BETWEEN THE MIXED-MODE S PARAMETERS AND
COUPLER CHARACTERISTICS

Para-meters	Characteristics			
	Quadrature Type 1	Quadrature Type 2	Rat-race Type 1	Rat-race Type 2
S_{ddAA}	Differential Port A matching performance			
S_{ddBB}	Differential Port B matching performance			
S_{ddAB}	Coupling between A and B	Isolation between A and B	Isolation between Σ and Δ ports	Transmission between Δ and B
S_{dsAC}	Transmission between A and C	Transmission between A and C	Transmission between Δ and C	Transmission between Δ and C
S_{dsAD}	Isolation between A and D	Coupling between A and D	Transmission between Δ and D	Isolation between Σ and Δ ports
S_{dsBC}	Isolation between B and C	Coupling between B and C	Transmission between Σ and C	Isolation between two inputs
S_{dsBD}	Transmission between B and D	Transmission between B and D	Transmission between Σ and D	Transmission between Σ and B
S_{ssCC}	Single-ended Port C matching performance			
S_{ssDD}	Single-ended Port D matching performance			
S_{ssCD}	Coupling between C and D	Isolation between C and D	Isolation between two inputs	Transmission between Σ and C
S_{ccAA}	Common-mode reflection at A			
S_{ccBB}	Common-mode reflection at B			
S_{ccAB}	Common-mode transmission from A to B			
S_{dcAA}	Differential-mode-to- common-mode conversion at A			
S_{dcBB}	Differential-mode-to- common-mode conversion at B			
S_{dcAB}	Differential-mode-to-common-mode conversion from A to B			
S_{csAC}	Response at A when Common-mode excited at C			
S_{csAD}	Response at A when Common-mode excited at D			
S_{csBC}	Response at B when Common-mode excited at C			
S_{csBD}	Response at B when Common-mode excited at D			

and 4. Since this port definition is valid for all the proposed types of couplers, the mixed-mode S matrices of the four types share identical forms. The method in [23] is employed for the conversions between the standard and mixed-mode S parameters. First, we give the port-definition matrices M:

$$M = \frac{1}{\sqrt{2}} \begin{pmatrix} 1 & -1 & 0 & 0 & 0 & 0 \\ 1 & 1 & 0 & 0 & 0 & 0 \\ 0 & 0 & 0 & 1 & -1 & 0 \\ 0 & 0 & 0 & 1 & 1 & 0 \\ 0 & 0 & \sqrt{2} & 0 & 0 & 0 \\ 0 & 0 & 0 & 0 & 0 & \sqrt{2} \end{pmatrix}. \quad (1)$$

Then, the mixed-mode S parameters (represented by S^{mm}) are obtained by using the following conversion:

$$[S^{mm}] = [M][S^{std}][M]^{-1}, \quad (2)$$

where S^{std} represents the single-ended S matrices, and $[M]^{-1}$ represents the inversed matrix M.

The form of S^{mm} can be written as:

$$\begin{pmatrix} S_{ddAA} & S_{dcAA} & S_{ddAB} & S_{dcAB} & S_{dsAC} & S_{dsAD} \\ S_{cdAA} & S_{ccAA} & S_{cdAB} & S_{ccAB} & S_{csAC} & S_{csAD} \\ S_{ddBA} & S_{dcBA} & S_{ddBB} & S_{dcBB} & S_{dsBC} & S_{dsBD} \\ S_{cdBA} & S_{ccBA} & S_{cdBB} & S_{ccBB} & S_{csBC} & S_{csBD} \\ S_{sdCA} & S_{scCA} & S_{sdCB} & S_{scCB} & S_{ssCC} & S_{ssCD} \\ S_{sdDA} & S_{scDA} & S_{sdDB} & S_{scDB} & S_{ssDC} & S_{ssDD} \end{pmatrix}, \quad (3)$$

where the first and second letters of the subscripts denotes the response and stimulus modes, respectively, and the letter "d", "c" and "s" represents the differential, common and

single-ended modes, respectively. As mentioned above, all the expected mixed-mode S matrices are identical in forms as (3). According to the port definition of the four coupler types (Figs. 3(a)–4(b)), each of the mixed-mode S parameters represents one characteristic of its corresponding coupler, as tabulated in Table I.

B. The Quadrature Coupler Type 1

As demonstrated in Fig. 3(a), the input, through, coupled, and isolated ports are defined clockwise as ports A, C, B, and D, respectively. This coupler type has two uses: (i) a balanced input with a balanced-coupled and unbalanced-through output, while the other unbalanced port being isolated; and (ii) inputing at an unbalanced port and outputting at unbalanced and balanced ports, with the other balanced port being isolated. This type of schematic corresponds to the topologies I and II illustrated in Fig. 1(a), which realizes the balanced/unbalanced to balanced-unbalanced-mixed operation.

According to Fig. 3(a), the Y matrix of the circuit (represented by Y_{cir}) is given as

$$[Y_{cir}] = \begin{pmatrix} x_1 & x_2 & jY_2 & 0 & 0 & 0 \\ x_2 & x_3 & 0 & 0 & 0 & jY_1 \\ jY_2 & 0 & 0 & jY_4 & 0 & 0 \\ 0 & 0 & jY_4 & x_4 & x_5 & 0 \\ 0 & 0 & 0 & x_5 & x_6 & jY_3 \\ 0 & jY_1 & 0 & 0 & jY_3 & 0 \end{pmatrix}, \quad (4)$$

where Y_i ($i = 1, 2, 3, 4$) are the admittances of the characteristic impedances Z_i ($i = 1, 2, 3, 4$), respectively. The entries x_i ($i = 1, 2, 3, 4, 5, 6$) are given by

$$x_1 = -j(Y_2 \cot \frac{\theta}{2} + Y_{g1} \cot \theta); \quad (5)$$

$$x_2 = jY_{g1} \csc \theta; \quad (6)$$

$$x_3 = -j(Y_1 \cot \frac{\theta}{2} + Y_{g1} \cot \theta); \quad (7)$$

$$x_4 = -j(Y_4 \cot \frac{\theta}{2} + Y_{g2} \cot \theta); \quad (8)$$

$$x_5 = jY_{g2} \csc \theta; \quad (9)$$

$$x_6 = -j(Y_3 \cot \frac{\theta}{2} + Y_{g2} \cot \theta), \quad (10)$$

where θ is the electrical length of the $\lambda/2$ lines. The detailed derivation of Y parameters is given in Appendix A.

Then, the standard S parameters of the circuit is converted from Y_{cir} using the following formula [24]:

$$[S_{cir}^{std}] = \lim_{\theta \to \pi} ([U] - [\sqrt{z}][Y_{cir}][\sqrt{z}])([U] + [\sqrt{z}][Y_{cir}][\sqrt{z}])^{-1}, \quad (11)$$

where $[\sqrt{z}]$ is a diagonal matrix comprising the square roots of the terminated impedances R_i ($i = A, B, C, D$) as given by:

$$\begin{pmatrix} \sqrt{R_A} & 0 & 0 & 0 & 0 & 0 \\ 0 & \sqrt{R_A} & 0 & 0 & 0 & 0 \\ 0 & 0 & \sqrt{R_C} & 0 & 0 & 0 \\ 0 & 0 & 0 & \sqrt{R_B} & 0 & 0 \\ 0 & 0 & 0 & 0 & \sqrt{R_B} & 0 \\ 0 & 0 & 0 & 0 & 0 & \sqrt{R_D} \end{pmatrix}. \quad (12)$$

Note that, the limit operation is utilized for manipulating the matrix containing ∞ elements.

Following this, the mixed-mode S matrix of the circuit can be extracted using equation (2), which can be expressed as:

$$S_{cir}^{mm} = \frac{1}{N} \begin{pmatrix} \alpha & 0 & \beta & 0 & \gamma & \delta \\ 0 & -1 & 0 & 0 & 0 & 0 \\ \beta & 0 & \epsilon & 0 & \zeta & \eta \\ 0 & 0 & 0 & -1 & 0 & 0 \\ \gamma & 0 & \zeta & 0 & \iota & \kappa \\ \delta & 0 & \eta & 0 & \kappa & \mu \end{pmatrix}. \tag{13}$$

Limited by the page space, the expanded expression is not given due to its complicated form.

According to the coupler's operation as in [20] and considering the port configuration of Fig. 3(a), the mixed-mode S parameters should satisfy the matching condition:

$$S_{ddAA} = S_{ddBB} = S_{ssCC} = S_{ssDD} = 0, \tag{14}$$

the isolation condition:

$$S_{dsAD} = S_{dsBD} = 0, \tag{15}$$

and the quadrature and power-division conditions:

$$S_{dsAC}/S_{ddAB} = S_{dsBD}/S_{ssCD} = jk. \tag{16}$$

Comparing equations (3) and (13) and combing equations (14)–(16), we obtain the following:

$$\alpha = \delta = \epsilon = \zeta = \iota = \mu = 0; \tag{17}$$

$$\gamma/\beta = \eta/\kappa = jk. \tag{18}$$

Solving (17) and (18) leads to the final solutions for the characteristic impedances, which are given by:

$$Z_1 = \frac{k\sqrt{R_A R_D}}{\sqrt{2}}, \tag{19}$$

$$Z_2 = \frac{k\sqrt{R_A R_C}}{\sqrt{2(k^2+1)}}, \tag{20}$$

$$Z_3 = \frac{k\sqrt{R_B R_D}}{\sqrt{2(k^2+1)}}, \tag{21}$$

$$Z_4 = \frac{k\sqrt{R_B R_C}}{\sqrt{2}}. \tag{22}$$

Inspecting the final equations, the impedances of the $\lambda/2$ lines are undetermined. This will be discussed later.

C. The Quadrature Coupler Type 2

The second type of the quadrature coupler is shown as Fig. 3(b), which corresponds to III and IV topologies shown in Fig. 1(a). This type has balanced input/isolation and two unbalanced outputs, and the roles of input/isolation and output can be exchanged due to the nature of branch-line couplers. Therefore, this type realizes balanced to unbalanced operation,

and vice versa. The procedure for the analysis is similar to the one in the previous subsection. First, we give the Y matrix as:

$$[Y_{cir}] = \begin{pmatrix} x_1 & x_2 & jY_2 & 0 & 0 & 0 \\ x_2 & x_3 & 0 & 0 & jY_1 & 0 \\ jY_2 & 0 & 0 & 0 & 0 & jY_4 \\ 0 & 0 & 0 & x_4 & x_5 & jY_3 \\ 0 & jY_1 & 0 & x_5 & x_6 & 0 \\ 0 & 0 & jY_4 & jY_3 & 0 & 0 \end{pmatrix}, \tag{23}$$

where

$$x_1 = -j(Y_2 \cot \frac{\theta}{2} + Y_{g1} \cot \theta); \tag{24}$$

$$x_2 = jY_{g1} \csc \theta; \tag{25}$$

$$x_3 = -j(Y_1 \cot \frac{\theta}{2} + Y_{g1} \cot \theta); \tag{26}$$

$$x_4 = -j(Y_3 \cot \frac{\theta}{2} + Y_{g2} \cot \theta); \tag{27}$$

$$x_5 = jY_{g2} \csc \theta; \tag{28}$$

$$x_6 = -j(Y_1 \cot \frac{\theta}{2} + Y_{g2} \cot \theta). \tag{29}$$

The mixed-mode S matrix is then obtained in the form of (13). Since ports A, B, C, and D are input, isolated, through, and coupled ports, respectively, the mixed-mode S parameters satisfy the isolation condition:

$$S_{ddAB} = S_{ssCD} = 0, \tag{30}$$

the quadrature and power-division conditions:

$$S_{dsAC}/S_{dsAD} = S_{sdCA}/S_{sdCB} = jk, \tag{31}$$

and the matching condition as equation (14).

Therefore, the following equation group is obtained:

$$\alpha = \beta = \epsilon = \iota = \kappa = \mu = 0; \tag{32}$$

$$\gamma/\delta = \gamma/\zeta = jk. \tag{33}$$

The final solutions for the characteristic impedances are given by:

$$Z_1 = \frac{k\sqrt{R_A R_B}}{2}, \tag{34}$$

$$Z_2 = \frac{k\sqrt{R_A R_C}}{\sqrt{2(k^2+1)}}, \tag{35}$$

$$Z_3 = \frac{k\sqrt{R_B R_D}}{\sqrt{2(k^2+1)}}, \tag{36}$$

$$Z_4 = k\sqrt{R_C R_D}. \tag{37}$$

Knowing the parameters k and R_i ($i = A, B, C, D$) with regard to the design specifications, the unknown parameters, namely, the line impedances, can be extracted simply using equations (34)–(37).

D. The Rat-Race Coupler Type 1

This type of rat-race coupler comprises balanced Σ and Δ ports and unbalanced input ports, see Fig. 4(a). Due to the rat-race nature, this type also support operating with unbalanced Σ/Δ ports and balanced input ports. This type corresponds to topologies I and II in Fig. 1(b). Similar to the quadrature couplers, we need to determine the Y matrix as given by:

$$[Y_{\text{cir}}] = \begin{pmatrix} x_1 & x_2 & jY_1 & 0 & 0 & 0 \\ x_2 & x_3 & 0 & 0 & 0 & jY_2 \\ jY_1 & 0 & 0 & -jY_3 & 0 & 0 \\ 0 & 0 & -jY_3 & x_4 & x_5 & 0 \\ 0 & 0 & 0 & x_5 & x_4 & jY_1 \\ 0 & jY_2 & 0 & 0 & jY_1 & 0 \end{pmatrix}, \quad (38)$$

where

$$x_1 = -j(Y_1 \cot \frac{\theta}{2} + Y_{g1} \cot \theta); \quad (39)$$

$$x_2 = jY_{g1} \csc \theta; \quad (40)$$

$$x_3 = -j(Y_2 \cot \frac{\theta}{2} + Y_{g1} \cot \theta); \quad (41)$$

$$x_4 = -j(-Y_3 \cot \frac{\theta}{2} + Y_{g2} \cot \theta); \quad (42)$$

$$x_5 = jY_{g2} \csc \theta; \quad (43)$$

$$x_6 = -j(Y_4 \cot \frac{\theta}{2} + Y_{g2} \cot \theta). \quad (44)$$

It is then converted to the mixed-mode S matrix, which shares identical form with (13).

Applying the conditions for rat-race operation, a equation group can be established. The conditions are:

$$S_{ddAB} = S_{ssCD} = 0, \quad (45)$$

$$S_{dsAC}/S_{dsAD} = -k, \ S_{dsBD}/S_{dsBC} = k, \quad (46)$$

and (14), which derive:

$$\alpha = \beta = \epsilon = \iota = \kappa = \mu = 0; \quad (47)$$

$$\delta/\gamma = -k; \quad (48)$$

$$\eta/\zeta = k. \quad (49)$$

Its solutions in terms of the impedances are given by:

$$Z_1 = \frac{\sqrt{(1+k^2)\,R_A R_C}}{\sqrt{2}k}, \quad (50)$$

$$Z_2 = \frac{\sqrt{(1+k^2)R_A R_D}}{\sqrt{2}}, \quad (51)$$

$$Z_3 = \frac{\sqrt{(1+k^2)R_B R_C}}{\sqrt{2}}, \quad (52)$$

$$Z_4 = \frac{\sqrt{(1+k^2)\,R_B R_D}}{\sqrt{2}k}. \quad (53)$$

It is seen that the power-division ratio k and terminated impedances R_i ($i = A, B, C, D$) determine the values of line impedances.

E. The Rat-Race Coupler Type 2

Eventually, the topologies III and IV in Fig. 1(b) are involved, corresponding to the schematic shown in Fig. 4(b). This type is different from the rat-race Type 1, since it possesses mixed input ports and Δ/Σ ports. This section only discusses the case with the balanced Σ port, since the analysis is very similar to the one with the balanced Δ.

The Y matrix of this type is given by:

$$[Y_{\text{cir}}] = \begin{pmatrix} x_1 & x_2 & jY_2 & 0 & 0 & 0 \\ x_2 & x_3 & 0 & 0 & 0 & jY_4 \\ jY_2 & 0 & 0 & 0 & jY_1 & 0 \\ 0 & 0 & 0 & x_4 & x_5 & -jY_3 \\ 0 & 0 & jY_1 & x_5 & x_6 & 0 \\ 0 & jY_4 & 0 & -jY_3 & 0 & 0 \end{pmatrix}, \quad (54)$$

with

$$x_1 = -j(Y_2 \cot \frac{\theta}{2} + Y_{g1} \cot \theta); \quad (55)$$

$$x_2 = jY_{g1} \csc \theta; \quad (56)$$

$$x_3 = -j(Y_1 \cot \frac{\theta}{2} + Y_{g1} \cot \theta); \quad (57)$$

$$x_4 = -j(Y_3 \cot \frac{\theta}{2} + Y_{g2} \cot \theta); \quad (58)$$

$$x_5 = jY_{g2} \csc \theta; \quad (59)$$

$$x_6 = -j(Y_1 \cot \frac{\theta}{2} + Y_{g2} \cot \theta), \quad (60)$$

where the corresponding mixed-mode S matrix is the same as (13).

The matching, isolation, and rat-race conditions for this type are given by

$$S_{ddAB} = S_{ssCD} = 0, \quad (61)$$

and

$$S_{dsAD}/S_{dsAC} = k, \ S_{dsBD}/S_{dsBC} = -k, \quad (62)$$

and the equation (14).

Substitute (13) into the four conditions (14), (61) and (62), the following equation group could be established:

$$\alpha = \beta = \epsilon = \iota = \kappa = \mu = 0; \quad (63)$$

$$\delta/\gamma = k; \quad (64)$$

$$\eta/\zeta = -k. \quad (65)$$

Finally, the solutions in impedance forms are given by:

$$Z_1 = \frac{\sqrt{(1+k^2)\,R_A R_B}}{2}, \quad (66)$$

$$Z_2 = \frac{\sqrt{(1+k^2)\,R_A R_C}}{\sqrt{2}k}, \quad (67)$$

$$Z_3 = \frac{\sqrt{(1+k^2)\,R_B R_D}}{\sqrt{2}k}, \quad (68)$$

$$Z_4 = \sqrt{(1+k^2)\,R_C R_D}. \quad (69)$$

Besides, to obtain a coupler with the balanced Δ port, we simply swap the lengths of Z_1 and Z_4, and the impedance equations (66)–(69) remain unchanged.
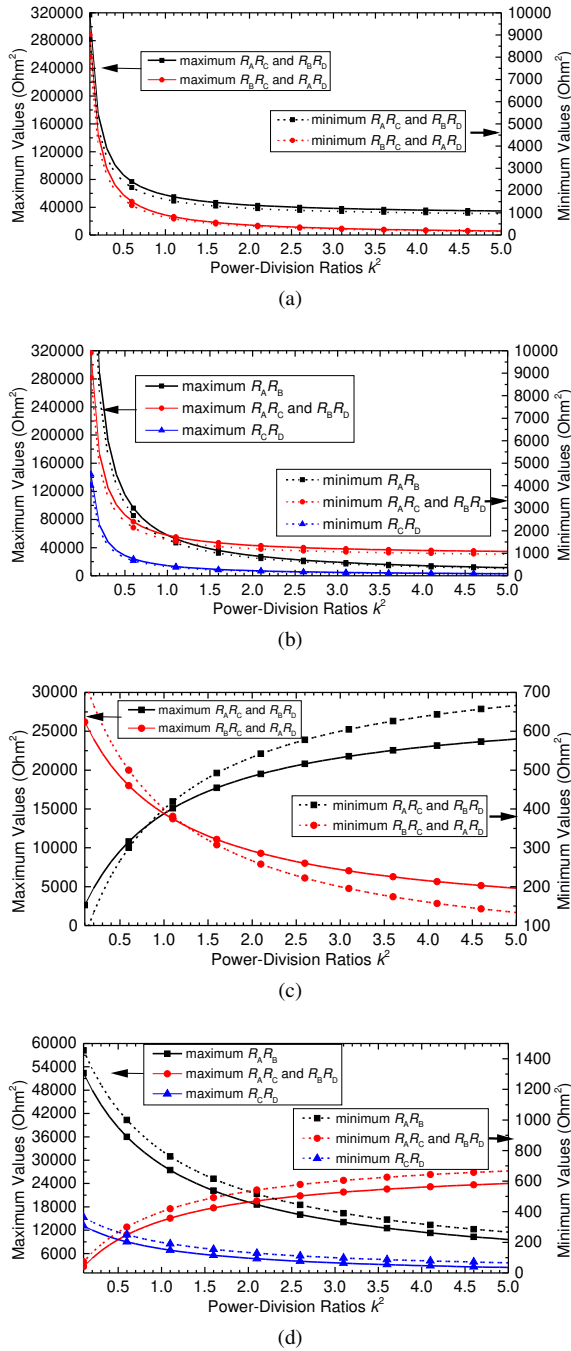
(a)

(b)

(c)

(d)

Fig. 5. Maximum and minimum values of $R_m R_n$ $(m, n = A, B, C, D)$ versus power-division ratios k^2 for (a) Quadrature type 1, (b) Quadrature type 2, (c) Rat-race type 1, and (d) Rat-race type 2.

III. THE PARAMETER ANALYSIS AND DESIGN GUIDE

A. The Restrictions of Power-Division Ratio and Terminated Resistances

According to equations (19)–(22), (34)–(37), (50)–(53), and (66)–(69), the power-division ratios k and terminated resistances $R_{A,B,C,D}$ can be arbitrary. However, in practical, the implemented power-division ratios and terminated resistances are limited by the used technology. Since the design equations are in closed-form, it is easy to obtain the available values of k and $R_{A,B,C,D}$.

For most microstrip fabrication technologies, the implementable line impedances are from about $20 \, \Omega$ to $120 \, \Omega$. Figs. 5(a)–5(d) demonstrate the maximum and minimum values of $R_m R_n$ $(m, n = A, B, C, D)$ with various k^2. For example, if we would like to design a quadrature coupler with type-1 configuration and 2:1 power division, the available values of $R_A R_C \backslash R_B R_D$ and $R_A R_D \backslash R_B R_C$ are $1200 - 43200 \, \Omega^2$, $400 - 14400 \, \Omega^2$, respectively.

B. The Selection of Two $\lambda/2$ Lines

The aforementioned derivations are based on the center frequency where the electrical lengths of the lines are $\lambda/4$, $\lambda/2$ or $3\lambda/4$. The impedances of the two $\lambda/2$ lines are not included in the design equations. However, their values may affect the performance at other frequencies except the center frequency. Therefore, following extraction of the parameters at center frequencies, the effects of Z_{g1} and Z_{g2} need to be investigated.

The effects of the two $\lambda/2$ lines can be generally summarized to two aspects. One is the effect on common-mode suppressions, and the other is the effect on differential-mode and differential-to-single-ended performance. The most effective and straightforward approach is utilizing a simulation software to calculate the mixed-mode S parameters over a certain frequency range, and the frequency range is set as dc to the second harmonic, which is sufficient to characterize this circuit. By tuning the values of Z_{g1} and Z_{g2} and observing the S-parameters variation, the final set of the values could be determined.

We take the prototype of quadrature type 1 with $k = 2$ and $R_A = R_B = R_C = R_D = 50 \, \Omega$ for example. At the center frequency, when the balanced port A is set as the input, the power-division ratio at ports C and B is 6 dB and the corresponding phase difference is $90°$ as shown in Figs. 6(a) and 6(b), thus revealing a 4:1 power division and quadrature operation. Meanwhile, when the unbalanced port D is the input, the 6-dB power-division ratio and $90°$ phase difference are observed at ports C and B. From Figs. 6(a)–6(f), ideal matching, isolation and common-mode suppression are obtained at the center frequency.

For simplifying the analysis, the values of Z_{g1} and Z_{g2} are assumed to be equal, *i.e.*, $Z_{g1} = Z_{g2} = Z_g$. Selecting different sets of Z_g, we calculated the mixed-mode S parameters over the frequency range from dc to the second harmonic. Since this circuit is a coupler applied in differential systems, the parameters we focus on are the differential-mode parameters, the common-mode suppression, and the differential-to-common-mode conversion, as tabulated in Table I.

From Fig. 6(a), when the value of Z_g increases from 20 to $120 \, \Omega$, the flatness of the power-division ratio S_{dsAC}/S_{ddAB} and S_{sdDB}/S_{ssDC} are degraded. The phase-difference performance shows a similar trend when values of Z_g increases from 20 to $120 \, \Omega$, as shown in Fig. 6(b). Meanwhile, the port matching, isolation and common-mode suppression performances are illustrated in Figs. 6(c), 6(d) and 6(e). To evaluate the bandwidths, the maximum value is set as -10 dB. When Z_g increases, the fractional bandwidth (FBW) of matching
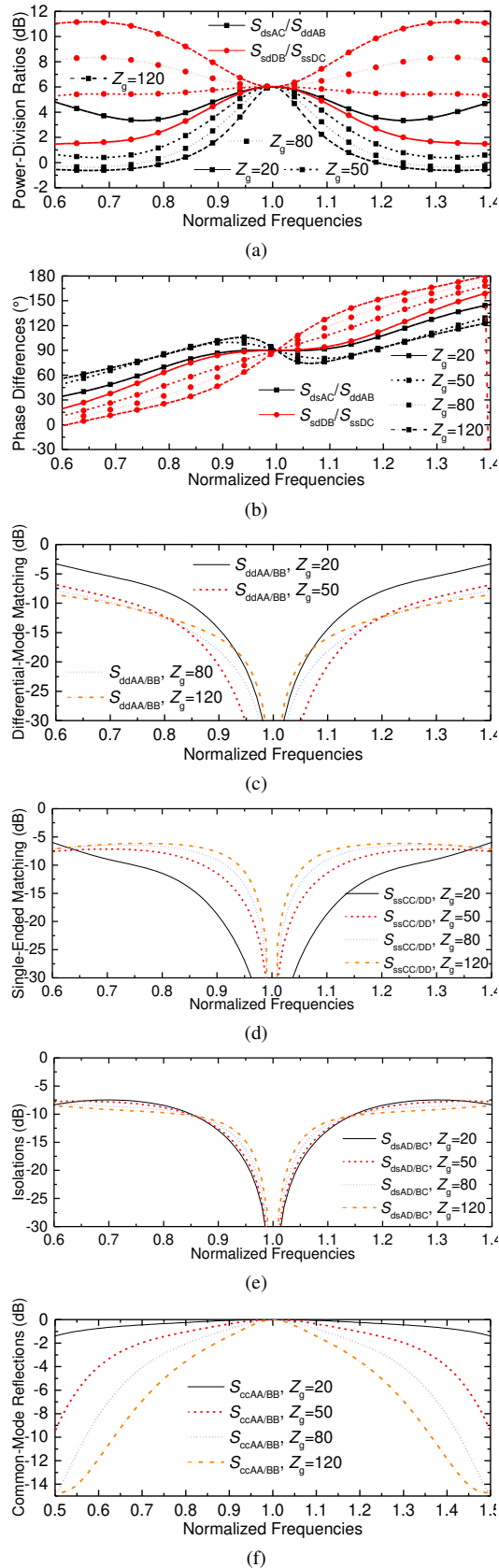
(a)

(b)

(c)

(d)

(e)

(f)

Fig. 6. Calculated mixed-mode S parameters of the Quadrature Type 1 versus different sets of Z_g: (a) Power divisions; (b) Phase differences; (c) Differential-mode matchings; (d) Single-ended matchings; (e) Isolations; (f) Common-mode reflections.

TABLE II
ELECTRICAL PARAMETERS FOR THE FOUR PROTOTYPES

Param-eters	Quadrature		Rat-Race	
	Type 1	*Type 2*	*Type 1*	*Type 2*
k^2	4	3	2	3
$R_A (\Omega)$	75	75	75	50
$R_B (\Omega)$	100	100	100	50
$R_C (\Omega)$	50	50	50	50
$R_D (\Omega)$	60	60	60	50
$Z_1 (\Omega)$	94.9	75	53.0	50
$Z_2 (\Omega)$	38.7	37.5	82.2	40.8
$Z_3 (\Omega)$	49.0	47.4	86.6	40.8
$Z_4 (\Omega)$	100	94.9	67.1	50
$Z_{t1} (\Omega)$	33	20	20	20
$Z_{t2} (\Omega)$	44	20	20	20

at the balanced ports $S_{ddAA/BB}$ becomes wider, whereas the bandwidths of the single-ended matching $S_{ssCC/DD}$ are getting narrower. Differently, when Z_g varies, the isolation $S_{dsAD/BC}$ remains almost unchanged.

As for the common-mode suppression, we expect that all the input common-mode powers are totally reflected, *i.e.*, no power transmitted to other ports or converted to differential-mode and single-ended signals. Therefore, it is sufficient to only focus on the common-mode reflection $S_{ccAA/BB}$. According to [3, Table 1], it can be said that the common-mode signals are completely rejected when the transmissions are suppressed below -15 dB for most of applications. In this paper, the common-mode signals input from a balanced port (port A, for example) are converted to five parts, including the differential-mode response at the input balanced port (S_{dcAA}), the common- and differential-mode responses at the output balanced port (S_{ccBA} and S_{dcBA}), and the single-ended responses at two unbalanced ports (S_{scCA} and S_{scDA}). If all of the transmissions are suppressed below -15 dB, the reflection (S_{ccAA}) will be greater than -0.7 dB, which means that 85% common-mode powers are reflected. Therefore, in this paper, we set -0.7 dB as the minimum common-mode reflection for completely suppressing common-mode signals. From Fig. 6(f), the FBW of the common-mode reflection ($S_{ccAA/BB}$) varies from 14% to 78% when Z_g deceases from 120 Ω to 20 Ω.

It can be observed from the simulation example that when the $\lambda/2$-line impedances increase, the bandwidths of power divisions, phase differences, single-ended matchings, isolations and common-mode reflections are getting narrower. However, the bandwidths of the differential-mode matchings become wider. Therefore, when selecting the optimized Z_{g1} and Z_{g2}, there might be trade-offs considering the different bandwidth performance.

C. The Design Procedure

Finally, the overall design procedure for the coupler can be summarized as the following steps:

1) Select a proper type of the quadrature or the rat-race coupler, based on the required port configurations.
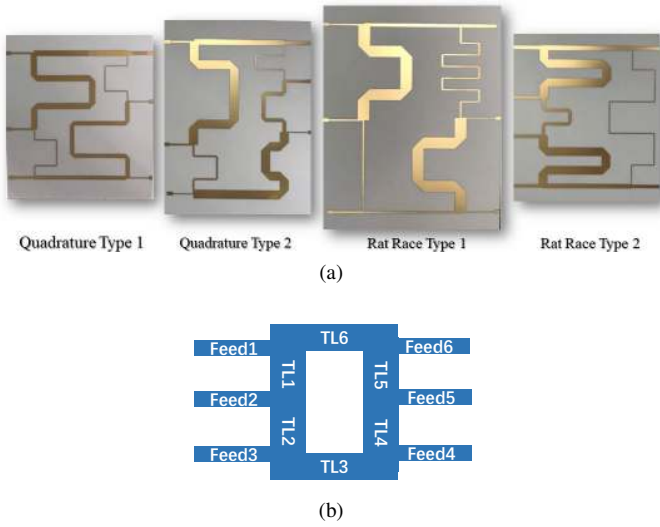
(a)

(b)

Fig. 7. Fabricated prototypes with microstrip technology: (a) Photograph, (b) Line definition for expressing layout dimension.

2) According to the application specification, determine the power-division ratios k^2, terminated impedances R_m $(m = A, B, C, D)$, operation bandwidths and common-mode-rejection bandwidths.

3) Calculate the line impedances using the derived equations (19)–(22), (34)–(37), (50)–(53), or (66)–(69).

4) Simulate the mixed-mode S parameters using ideal circuit models, as illustrated in Figs. 6(a)–6(f). Then, considering the specifications of both operation and common-mode-rejection bandwidths, determined the final impedances of the two $\lambda/2$ lines by tunning the Z_{g1} and Z_{g2} values.

IV. SIMULATIONS AND EXPERIMENTS

For the purpose of verification, four prototypes covering the four coupler types were designed and fabricated based on the microstrip technology, the substrates of which were chosen as Rogers RO4350B with permittivity $\varepsilon_r = 3.66$ and thickness of 0.76 mm . The operating frequencies for all four prototypes are centered at 1 GHz, and all the key design specifications and the calculated parameter are given in Table. II. Finally, the prototypes were fabricated using the printed circuit board (PCB) technology, and their photographs are shown in Fig. 7(a). The physical dimensions are given in Table III, where the mapping of the microstrip lines are shown in Fig. 7(b). The measurements were excuted using R&S ZNBT8-24Port vector network analyzer, and SMA connectors were de-embedded for removing the mismatch caused by the 50-Ω SMA connectors under non-50-Ω ports (For more details of the de-embedding technique, please see Appendix B.) The measured results are shown in the upper bisection of each subfigures in Figs. 8–11. For comparison, the predicted results simulated with ideal transmission-line models in Keysight Advance Design System are also shown in the lower section of each subfigures in Figs. 8–11.

For the first prototype of quadrature type 1, the expected power-division ratio is $k^2 = 4$ at the center frequency.

TABLE III
LAYOUT DIMENSIONS OF THE FOUR PROTOTYPES (UNIT: MM)

| Parameters		Quadrature		Rat-Race	
		Type 1	Type 2	Type 1	Type 2
TL1	Width	3.0	4.4	.8	4.4
	Length	93.0	86.0	85.0	85.0
TL2	Width	5.0	0.8	0.7	1.6
	Length	46.0	45.0	46.5	44.6
TL3	Width	1.8	4.4	1.0	4.4
	Length	46.3	42.6	46.5	85.0
TL4	Width	38.7	4.4	.8	2.3
	Length	49.0	43.0	85.0	44.0
TL5	Width	2.0	1.8	0.6	0.4
	Length	93.0	44.0	139.5	141
TL6	Width	0.4	0.5	1.6	2.3
	Length	46.0	46.0	46.5	44.0
Feed1*	Width	0.8	0.8	0.8	1.7
Feed2*	Width	0.8	0.8	0.8	1.7
Feed3*	Width	1.2	0.4	1.2	1.7
Feed4*	Width	0.4	0.4	0.4	1.7
Feed5*	Width	0.4	1.2	0.4	1.7
Feed6*	Width	1.7	1.7	1.7	1.7

*All of the lengths of the feedlines are 10 mm.

Observing the measured power-division ratios and phases in Figs. 8(a) and 8(b), respectively, at the center frequency of 1 GHz, when balanced port A is set as the input, k and the phase differences at ports C and B are about 6 dB and $89.5°$, respectively. This reveals a 4:1 power division and quadrature operation. Meanwhile, when the unbalanced port D is the input, the 6.0-dB power-division ratio and $91.8°$ phase difference are observed at ports C and B, see Figs. 8(a) and 8(b). When considering a 1-dB variation, the FBWs for the two power-division ratios are 34% and 20%, respectively. From Fig. 8(c), the differential return loss (S_{ddAA}, S_{ddBB}), single-ended return loss (S_{ssCC}, S_{ssDD}), and port isolations (S_{dsAD}, S_{dsBC}) are all greater than 20-dB at 1 GHz, where the corresponding FBW is 29% if the standard is set as -10 dB. For the common-mode rejection shown in Fig. 8(d), the predicted and measured common-mode reflections (S_{ccAA}, S_{ccBB}) are close to 0 dB at 1 GHz, while the other responses converted from common-mode stimuluses are all below -20 dB. If the minimum acceptable reflection is set as -0.7 dB, the common-mode signals are suppressed within 0.72 GHz–1.2 GHz, at both ports A and B. This reveals a 48% FBW. Within the common-mode-rejected band, the common-mode transmissions (S_{dcAB}, S_{csAC}, S_{csAD}, S_{csBC} and S_{csBD}) are all suppressed below -10 dB. All the measured results show slight deviations compared with the corresponding ideal mixed-mode S parameters plotted at the lower subfigures of Figs. 8(a)–8(d), which proves the design of quadrature type 1 to be valid and effective.
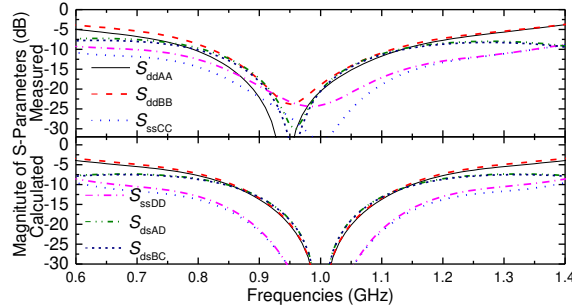
Subsequently, we evaluate the prototype for quadrature type 2, whose power-division ratio is 3:1. The measure and calculated results are exhibited in Fig. 9. From Fig. 9(a), the power-division ratio is 4.78 dB at 1 GHz, which is consistent
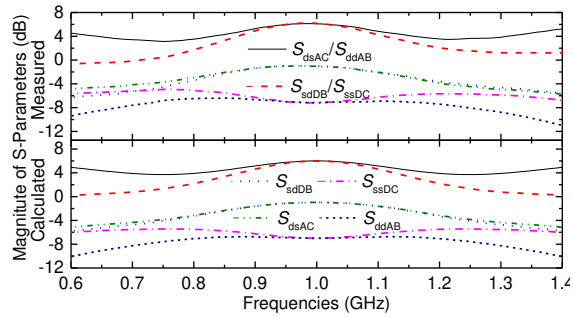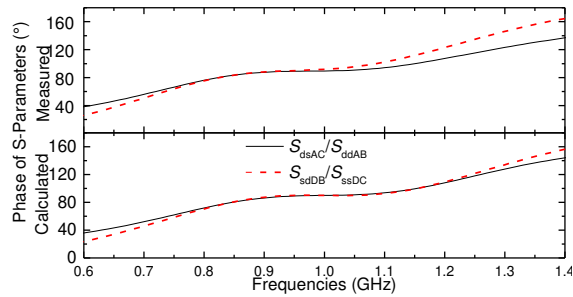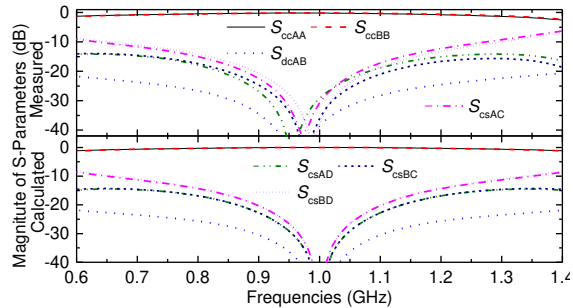
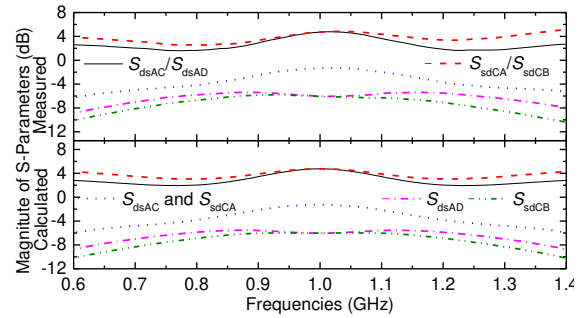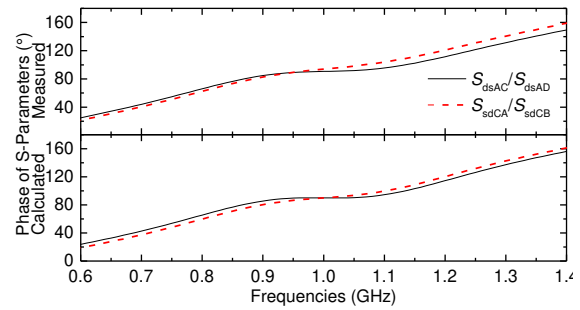Fig. 8. Measured and calculated ideal mixed-mode S parameters for the prototype of the quadrature type 1: (a) Power-division ratios; (b) Phase differences; (c) Port matching and isolation; (d) Common-mode suppression. The upper subfigures are the measured results while the lower ones are the ideal results.
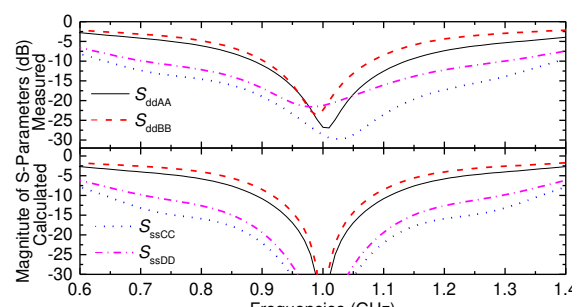

Fig. 9. Measured and calculated mixed-mode S parameters for the prototype of the quadrature type 2: (a) Power-division ratios; (b) Phase differences; (c) Port matching and isolation; (d) Common-mode suppression. The upper subfigures are the measured results while the lower subfigures are the ideal results.

with the 3:1 power division. The power-division ratios of ports A to C/D and C to A/B are 4.7 ± 1 dB within the frequency range of 0.91 GHz–1.12 GHz and 0.89 GHz–1.4 GHz, respectively, showing 21% and 51% FBWs. The corresponding phase differences shown in Fig. 9(b) are 90.7° and 89.9° at 1 GHz, and the phase differences deviate within
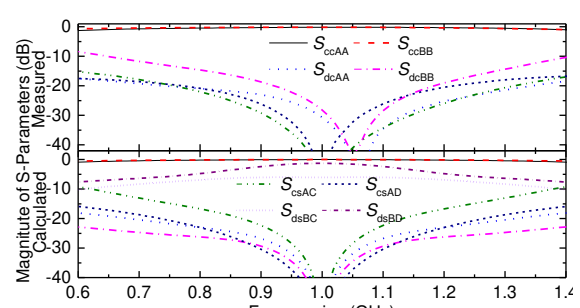
$\pm 3°$ in the range of $0.92 - 10.7$, showing a 15% FBW. From Fig. 9(c), the matching and isolation performances of all ports are below -10 dB in the frequency range of 0.9 GHz–1.08 GHz, showing 18% FBW. At last, for the common-mode suppression shown in Fig. 9(d), the reflection at ports A and B are larger than -0.7 dB in the frequency range of 0.72 GHz to 1.2 GHz, which indicates that the common-mode signals are
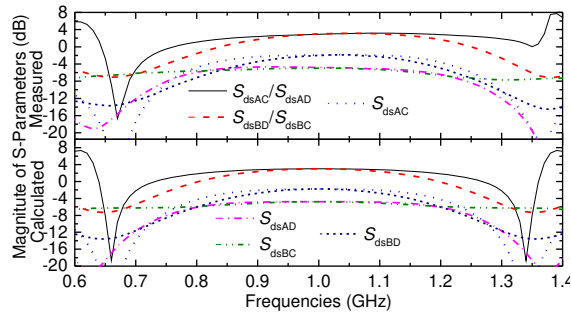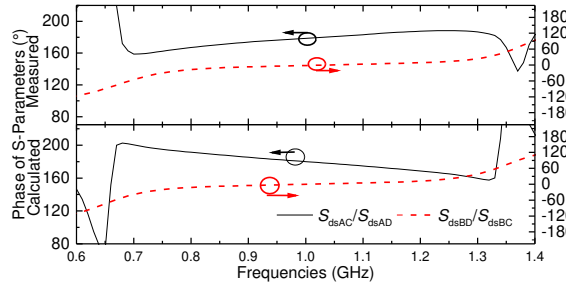
Fig. 10. Measured and calculated mixed-mode S parameters for the prototype of the rat-race type 1: (a) Power-division ratios; (b) Phase differences; (c) Port matching and isolation; (d) Common-mode suppression. The upper subfigures are the measured results while the lower ones are the ideal results.
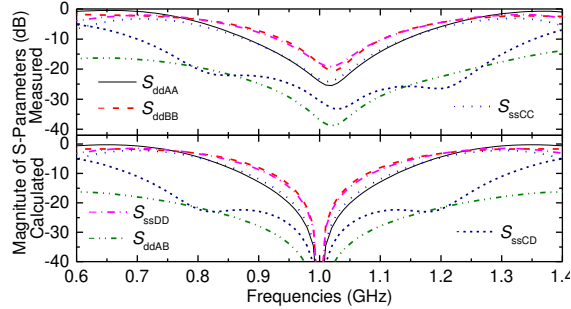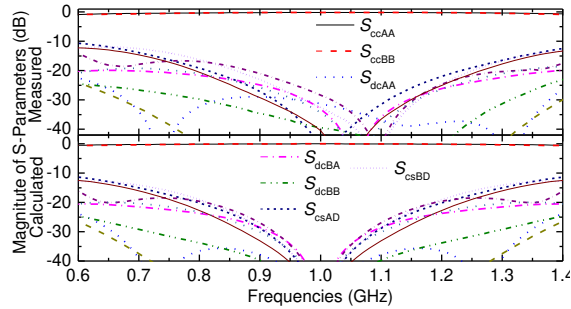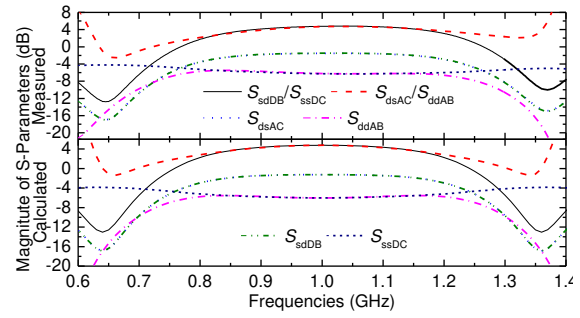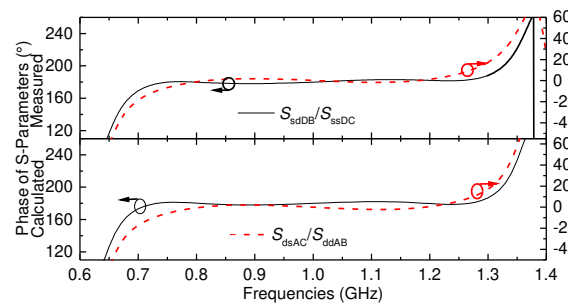

Fig. 11. Measured and calculated mixed-mode S parameters for the prototype of the rat-race type 2: (a) Power-division ratios; (b) Phase differences; (c) Port matching and isolation; (d) Common-mode suppression. The upper subfigures are the measured results while the lower ones are the ideal results.

sufficiently suppressed in the FBW of 57%. Compared with the ideal S parameters plotted at the lower subfigures, the measured values are almost the same, with small deviations caused by some unpredictable factors, such as microstrip discontinuities, fabrication errors, and board deformations.

Then from Fig. 10, the measured performances of the prototype for the rat-race type 1 can be evaluated. In detail, when ports A and B excited, the measured power-division ratios deviate from 3 dB by ±1 dB in the frequency range of 0.86 GHz–1.28 GHz and 0.92 GHz–1.18 GHz, respectively, showing 42% and 26% FBWs as depicted in Fig. 10(a). The phase performance is shown in Fig. 10(b). When the Δ (A) port is excited, the phase difference at ports C and D is $180\pm3°$ within the frequency range of 0.96 to 1.1 GHz, showing 14% FBW. When the Σ (B) port excited, the phase difference at

TABLE IV
SUMMARY FOR THE BANDWIDTH PERFORMANCE OF THE FOUR PROTOTYPES

Performance	Standard		Quadrature		Rat Race	
			Type 1	Type 2	Type 1	Type 2
Matching & Isolation	>10 dB	Range (GHz)	0.82—1.15	0.90—1.08	0.93—1.10	0.84—1.17
		FBW	33%	18%	17%	33%
Power Division 1	±1 dB	Range (GHz)	0.87—1.15 (S_{dsAC}/S_{ddAB})	0.91—1.12 (S_{dsAC}/S_{dsAD})	0.86—1.28 (S_{dsAC}/S_{dsAD})	0.87—1.18 (S_{sdDB}/S_{ssDC})
		FBW	28%	21%	42%	31%
Power Division 2	±1 dB	Range (GHz)	0.87—1.07 (S_{sdDB}/S_{ssDC})	0.89—1.40 (S_{sdCA}/S_{sdCB})	0.92—1.18 (S_{dsBD}/S_{dsBC})	0.87—1.18 (S_{dsAC}/S_{ddAB})
		FBW	20%	51%	26%	31%
Phase Difference 1	±3°	Range (GHz)	0.89—1.09 (S_{dsAC}/S_{dsAB})	0.92—1.07 (S_{dsAC}/S_{dsAD})	0.96—1.10 (S_{dsAC}/S_{dsAD})	0.73—1.20 (S_{sdDB}/S_{ssDC})
		FBW	20%	15%	14%	47%
Phase Difference 2	±3°	Range (GHz)	0.88—1.03 (S_{sdDB}/S_{ssDC})	0.92—1.07 (S_{sdCA}/S_{sdCB})	0.96—1.10 (S_{dsBD}/S_{dsBC})	0.77—1.23 (S_{dsAC}/S_{ddAB})
		FBW	15%	15%	14%	46%
Common-Mode Reflection	>-0.7 dB	Range (GHz)	0.72—1.2	0.78—1.35	0.62—1.40	0.79—1.27
		FBW	48%	57%	78%	48%
Overall	Intersection	Range (GHz)	0.89—1.03	0.91—1.07	0.96—1.10	0.87—1.17
		FBW	14%	16%	14%	30%

ports C and D is $0 \pm 3°$ in the frequency range of 0.96 to 1.1 GHz, showing 14% FBW. For the matching and isolation performances shown in Fig. 10(c), all the return losses at the ports are higher than 10 dB in the frequency range of 0.93 GHz–1.1 GHz. The corresponding FBW is 17%. For the common-mode rejection, all the common-mode reflections (S_{ccAA} and S_{ccBB}) are larger than -0.7 dB from 0.62 GHz to 1.4 GHz. It can be concluded that the common-mode rejection FBW is 78%. The corresponding ideal results are illustrated in the lower subfigures, showing a good match with the measured data.

The measured power-division ratios for the rat-race type 2 are shown in Fig. 11(a) with the balanced port A being set as the input. The power-division ratio is 4.7 ± 1 dB in the frequency range of 0.87 GHz–1.18 GHz, whose relative FBW is 31%. When port D excited, the power-division ratio is 4.7 ± 1 in the range of 0.87 GHz–1.18 GHz, with a relative FBW of 31%. Meanwhile, from Fig. 11(b), the phase differences are $0 \pm 3°$ from 0.73 GHz–1.2 GHz and $180 \pm 3°$ from 0.77 GHz–1.23 GHz with ports A and D being excited, respectively. The mixed-mode matching and isolation performance of the four ports are all below -10 dB in the frequency range of 0.84 GHz–1.17 GHz, which indicates that the matching and isolation FBW of this prototype is 33%. For the common-mode rejection, all the common-mode reflections (S_{ccAA} and S_{ccBB}) are larger than -0.7 dB from 0.79 GHz to 1.27 GHz. The corresponding relative FBW is 48%. The ideally-calculated results are plotted in the lower subfigures for comparison, showing a reasonable match with the measured results.

In general, all the measured results of the four prototypes agrees well with their design specifications. Therefore, it can be concluded that the design methodology proposed in this paper is valid and effective. To summarize, all the bandwidth performances of the four prototypes are tabulated in Table IV. From Table IV, the common-mode suppression bandwidths of the four configurations are different, but all of them are favorable. The good common-mode-rejection level might be due to the low impedances of the $\lambda/2$ lines. This is consistent with the analysis in Section III. Moreover, the differential-mode and differential-to-single-ended bandwidths of the rat-race-type-2 prototype is much wider than those of other prototypes. The most obvious difference between the prototypes is that the terminated resistances of the rat-race type 2 are identical. Therefore, the different terminated resistances of the three prototypes may account for the bandwidth degradation. However, the common-mode performance is not much affected by the terminated resistances.

In essence, the key for the common-mode rejection is the $\lambda/2$ lines sandwiched between the balanced ports. This could be inferred from the Y matrices in (4), (23), (38) and (54). When the Y matrices are converted to mixed-mode S matrices, the x_i ($i = 1, 2, ..., 6$) terms in Y matrices contribute to composing the S_{cc} terms, thus it is hoped that the x_i terms remain ∞ in a range as wide as possible. Hence, a wideband phase inverter helps to enhance the CM-suppression FBWs.

Moreover, compared with the conventional single-ended couplers, the circuit size is relatively large, which is mainly attributed to the long $\lambda/2$ lines. Considering both the common-mode suppression and miniaturization, the compact wideband phase inverters reported in [25]–[27] are good candidates for replacing the long $\lambda/2$ lines. However, it will not be considered in this paper, but might be investigated in the future work.

V. CONCLUSION

This paper presented a series of six-port couplers, which possess hybrid ports with balanced and unbalanced input/output. The innovation of this paper lies in proposing couplers of this kind, and both the quadrature and rat-race types were included. This paper outlined the detailed design formulas and methodology, for designing couplers with arbitrary power divisions and port resistances. We proposed and designed four prototypes of different balanced and unbalanced configurations, and fabricated and experimentally evaluated them. From the measured results, it was concluded that the proposed design methodology is valid and effective. Since the derivations and analyses were all based on the fundamental transmission-line theory, the proposed methodology is universal for a range of technologies, including but not limited to the PCB, IC, and LTCC.

APPENDIX A
THE DERIVATION FOR THE Y MATRICES

In this appendix, only the Y matrix of the schematic shown in Fig. 3(a) is discussed. The Y parameters are directly calculated by the definition:

$$Y_{ij} = \frac{I_i}{V_j}|_{V_k=0, \ k \neq j}, \tag{70}$$

where Y_{ij} can be determined by exciting port j with the voltage V_j with shourt-circuiting all other ports and measuring
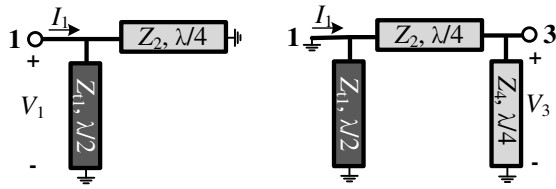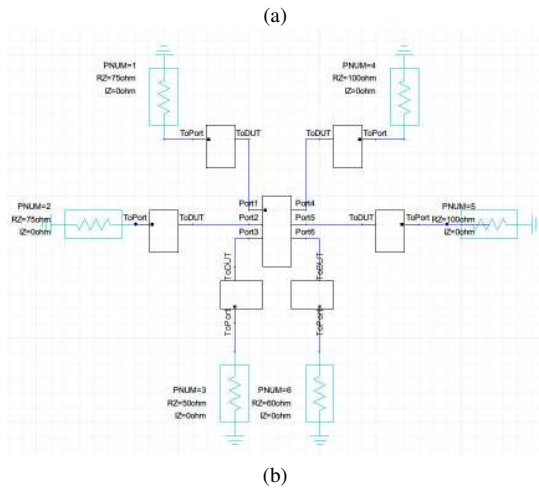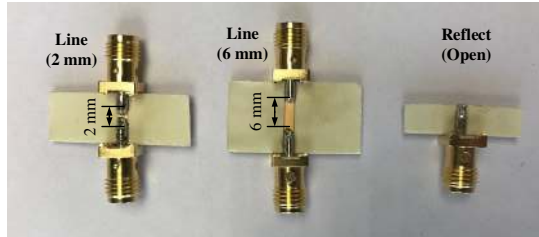
Fig. 12. Equivalent circuits when deriving Y_{11} (left) and Y_{13} (right).

(a)

(b)

Fig. 13. De-embedding technique: (a) PCBs for RTL de-embedding; (b) Schematic for de-embedding in ANSYS Electronics Desktop.

the short-circuited current at port j [20]. Considering port 1, there are only line Z_{g1} and Z_2 left when other ports are short circuited, as shown in the left part of Fig. 12. Hence, Y_{11} is actually the shunt impedance of the two short-circuited stubs, which is given by:

$$Y_{11} = -j(Y_{g1} \cot \pi + Y_2 \cot \frac{\pi}{2}). \tag{71}$$

The Y_{13} is derived by short-circuiting all the ports except port 3, and the equivalent circuit is given in the right port of Fig. 12. When voltage V_3 is applied at port 3, all the current I_1 will flow in line Z_2. Therefore, Y_{13} can be directly converted from the $ABCD$ parameters of line Z_2, which is given by:

$$\begin{pmatrix} A & B \\ C & D \end{pmatrix} = \begin{pmatrix} \cos \frac{\pi}{2} & jZ_2 \sin \frac{\pi}{2} \\ \frac{j}{Z_2} \sin \frac{\pi}{2} & \cos \frac{\pi}{2} \end{pmatrix}. \tag{72}$$

Using the conversion provided in [20], the final expression of Y_{13} is:

$$Y_{13} = \frac{BC - AD}{B} = jY_1 \csc \frac{\pi}{2}. \tag{73}$$
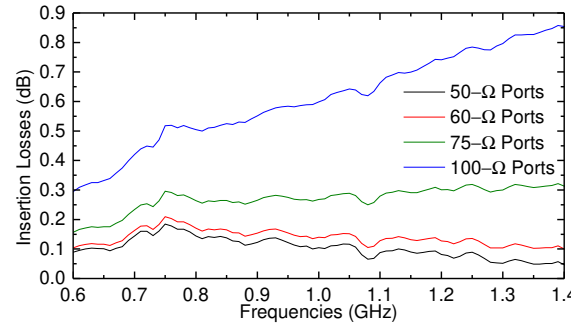
Other Y parameters can be derived with similar process.

Fig. 14. The insertion losses of SMA connectors when terminated with different resistances.
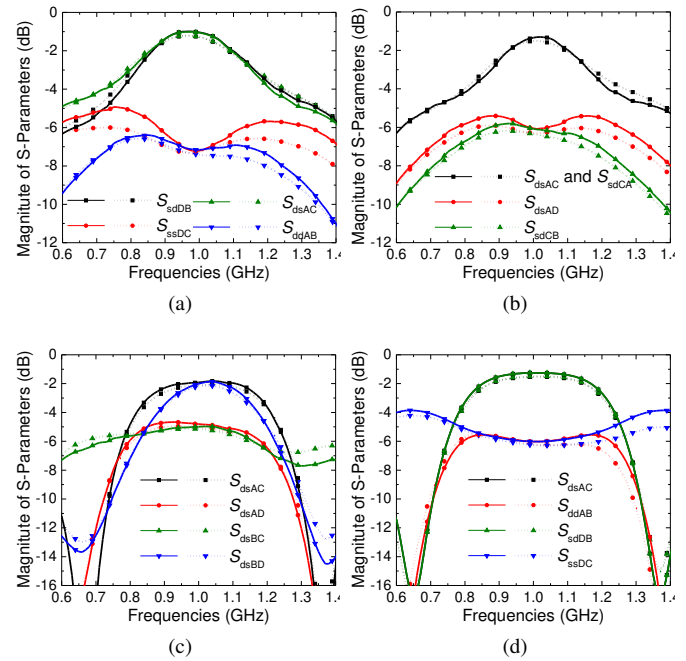

(a)

(b)

(c)

(d)

Fig. 15. Results with and without the de-embedding (represented by the solid and dotted curves, respectively) of (a) Quadrature type 1, (b) Quadrature type 2, (c) Rat-race type 1, and (d) Rat-race type 2.

APPENDIX B
HOW TO DE-EMBEDDING THE SMA CONNECTORS

The TRL (Thru-Reflection-Line) de-embedding method is used to remove the effects of SMA connectors. The steps are as follows.

1) Measure three PCBs: two boards with back-to-back SMA connectors and a sandwiched 6-mm and 2-mm lines, and one board with an open-ended SMA connector, as shown in Fig. 13(a).
2) Then, use the calibration wizard (Tools–>Calibration Wizard) in ANSYS Electronics Desktop (ANSYS Designer for older versions) to generate the s2p files for the SMA connectors corresponding to Port1 and Port2.
3) Use the 2port model in ANSYS Electronics Desktop with the exported fixture s2p files generated in the previous step, and set it as reciprocal model.
4) Use the nport model with the measured s6p files for the couplers, and cascade the 2port model generated

in the previous steps at each port. The corresponding schematic is shown in Fig. 13(b). After the running the linear analysis, the final measured results will be obtained with SMA connectors de-embedded.

Here, we composed Fig. 14 to demonstrate the SMAs' insertion losses with different termination resistances, which is obtained by the exported s2p files. It is observed that the insertion losses become larger when the terminated resistances deviate from 50 Ω gradually. This is reasonable because SMA connectors are used in 50–Ω systems. Furthermore, to evaluate the de-embedding effect, the transmission results before and after the de-embeddings are shown in Fig. 15. It is seen that the insertion loss and mismatch caused by the SMA connectors are effectively eliminated after the de-embedding process.

REFERENCES

[1] J.-X. Chen, Y. Zhan, W. Qin, Z.-H. Bao, and Q. Xue, "Analysis and design of balanced dielectric resonator bandpass filters," *IEEE Trans. Microw. Theory Techn.*, vol. 64, no. 5, pp. 1476–1483, May 2016.

[2] B. Zhang, Y. Wu, and Y. Liu, "Wideband single-ended and differential bandpass filters based on terminated coupled line structures," *IEEE Trans. Microw. Theory Techn.*, vol. 65, no. 3, pp. 761–774, Mar. 2017.

[3] W. Feng, W. Che, and Q. Xue, "The proper balance: overview of microstrip wideband balance circuits with wideband common mode suppression," *IEEE Microw. Mag.*, vol. 16, no. 5, pp. 55–68, Jun. 2015.

[4] B. Xia, L.-S. Wu, S.-W. Ren, and J.-F. Mao, "A balanced-to-balanced power divider with arbitrary power division," *IEEE Trans. Microw. Theory Techn.*, vol. 61, no. 8, pp. 2831–2840, Aug. 2013.

[5] W. Feng, H. Zhu, W. Che, and Q. Xue, "Wideband in-phase and out-of-phase balanced power dividing and combining networks," *IEEE Trans. Microw. Theory Techn.*, vol. 62, no. 5, pp. 1192–1202, May 2014.

[6] J. Shi, J. Qiang, K. Xu, Z.-b. Wang, L. Lin, J.-X. Chen, W. Liu, and X. Y. Zhang, "A balanced filtering branch-line coupler," *IEEE Microw. Wireless Compon. Lett.*, vol. 26, no. 2, pp. 119–121, Feb. 2016.

[7] J. Shi, J. Qiang, K. Xu, and J. X. Chen, "A balanced branch-line coupler with arbitrary power division ratio," *IEEE Trans. Microw. Theory Techn.*, vol. 65, no. 1, pp. 78–85, Jan. 2017.

[8] Y.-J. Huang and Y.-H. Pang, "Balanced-to-balanced rat-race coupler with bandpass response," in *2016 International Symposium on Antennas and Propagation (ISAP)*,. IEEE, 2016, pp. 902–903.

[9] Y. Zhou, H.-w. Deng, and Y. Zhao, "Compact balanced-to-balanced microstrip diplexer with high isolation and common-mode suppression," *IEEE Microw. Wireless Compon. Lett.*, vol. 24, no. 3, pp. 143–145, Mar. 2014.

[10] M. Arrawatia, M. S. Baghini, and G. Kumar, "Differential microstrip antenna for RF energy harvesting," *IEEE Trans. Antennas Propag.*, vol. 63, no. 4, pp. 1581–1588, Apr. 2015.

[11] Y. Yu and L. Sun, "A design of single-ended to differential-ended power divider for X band application," *Microwave Opt. Technol. Lett.*, vol. 57, no. 11, pp. 2669–2673, Nov. 2015.

[12] W. Zhang, Y. Liu, Y. Wu, A. Hasan, F. M. Ghannouchi, Y. Zhao, X. Du, and W. Chen, "Novel planar compact coupled-line single-ended-to-balanced power divider," *IEEE Trans. Microw. Theory Techn.*, vol. 65, no. 8, pp. 2953–2963, Aug. 2017.

[13] X. Gao, W. Feng, W. Che, and Q. Xue, "Wideband balanced-to-unbalanced filtering power dividers based on coupled lines," *IEEE Trans. Microw. Theory Techn.*, vol. 65, no. 1, pp. 86–95, Jan. 2017.

[14] W. Zhang, Y. Wu, Y. Liu, F. M. Ghannouchi, and A. Hasan, "A wideband balanced-to-unbalanced coupled-line power divider," *IEEE Microw. Wireless Compon. Lett.*, vol. 26, no. 6, pp. 410–412, Jun. 2016.

[15] W. Feng, M. Hong, M. Xun, and W. Che, "A novel wideband balanced-to-unbalanced power divider using symmetrical transmission lines," *IEEE Microw. Wireless Compon. Lett.*, vol. 27, no. 4, pp. 338–340, Apr. 2017.

[16] Q. Xue, J. Shi, and J.-X. Chen, "Unbalanced-to-balanced and balanced-to-unbalanced diplexer with high selectivity and common-mode suppression," *IEEE Trans. Microw. Theory Techn.*, vol. 59, no. 11, pp. 2848–2855, Nov. 2011.

[17] L. Jiao, Y. Wu, Z. Ning, W. Wang, and Y. Liu, "A new impedance-transforming dual-band balun with filtering response and favorable output isolations," *AEU - International Journal of Electronics and Communications*, vol. 71, pp. 162–167, Jan. 2017.

[18] H. Chu and J. X. Chen, "Dual-band substrate integrated waveguide balun bandpass filter with high selectivity," *IEEE Microw. Wireless Compon. Lett.*, vol. 24, no. 6, pp. 379–381, Jun. 2014.

[19] L. P. Feng and L. Zhu, "Wideband filtering balun on a novel hybrid multimode resonator with the functionality of vertical transition," *IEEE Trans. Compon. Packag. Manuf. Technol.*, vol. 7, no. 8, pp. 1324–1330, Aug. 2017.

[20] D. M. Pozar, *Microwave engineering*, 4th ed. Hoboken, NJ: Wiley, 2012.

[21] L. Jiao, Y. Wu, and Y. Liu, "Novel dual-band coupled-line quadrature couplers with unequal power division," *Electromagnetics*, vol. 36, no. 4, pp. 249–261, May 2016.

[22] Y. Wu, Q. Liu, S. W. Leung, Y. Liu, and Q. Xue, "A novel planar impedance-transforming tight-coupling coupler and its applications to microstrip baluns," *IEEE Trans. Compon. Packag. Manuf. Technol.*, vol. 4, no. 9, pp. 1480–1488, Sep. 2014.

[23] W. R. Eisenstadt, R. Stengel, and B. M. Thompson, *Microwave differential circuit design using mixed-mode S-parameters*, ser. Artech House microwave library. Boston: Artech House, 2006.

[24] P. Russer, *Electromagnetics, microwave circuit and antenna design for communications engineering*. Artech House, 2003.

[25] F. Lin, Q.-X. Chu, Z. Gong, and Z. Lin, "Compact broadband Gysel power divider with arbitrary power-dividing ratio using microstrip/slotline phase inverter," *IEEE Trans. Microw. Theory Techn.*, vol. 60, no. 5, pp. 1226–1234, Feb. 2012.

[26] H. T. Duong, H. V. Le, A. T. Huynh, N. Tran, and E. Skafidas, "Design of a compact ultra wideband balanced-to-balanced power divider/combiner," in *2013 Asia-Pacific Microwave Conference Proceedings (APMC)*, Nov. 2013, pp. 363–365.

[27] S. W. Y. Mung and W. S. Chan, "Wideband microstrip rat-race hybrid with via-swap phase inverter," *Electron. Lett.*, vol. 50, no. 2, pp. 96–98, Jan. 2014.